Dynamic water transport and droplet emergence in PEMFC gas diffusion layers

Aimy Bazylak, David Sinton, Ned Djilali *

Department of Mechanical Engineering, and Institute for Integrated Energy Systems, University of Victoria, Victoria, BC, Canada V8W 3P6

Abstract

The dynamics of liquid water transport through the gas diffusion layer (GDL) and into a gas flow channel are investigated with an *ex situ* experimental setup. Liquid water is injected through the bottom surface of the GDL, and the through-plane liquid pressure drop, droplet emergence and droplet detachment are studied. The dynamic behaviour of water transport in and on the surface of the GDL is observed through fluorescence microscopy, and the through-plane liquid pressure drop is measured with a pressure transducer. With an initially dry GDL, the initial breakthrough of liquid water in the GDL is preceded by a substantial growth of liquid water pressure. Post-breakthrough, droplets emerge with a high frequency, until a quasi-equilibrium liquid water pressure is achieved. The droplet emergence/detachment regime is followed by a transition into a slug formation regime. During the slug formation regime, droplets tend to pin near the breakthrough location, and the overall channel water content increases due to pinning and the formation of water slugs. Droplets emerge from the GDL at preferential breakthrough locations; however, these breakthrough locations change intermittently, suggesting a dynamic interconnection of water pathways within the GDL. The experiments are complemented by computational fluid dynamics (CFD) simulations using the volume of fluid method to illustrate the dynamic eruption mechanism.

1. Introduction

Proper water management is necessary for successful polymer electrolyte membrane fuel cell (PEMFC) operation. Although membrane hydration depends on water, an excess of liquid water leads to flooding in the catalyst layer, GDL, and gas flow channels. This can lead to fuel starvation and severe performance losses. Excess water in the fuel cell is also of concern with respect to freeze/thaw damage, start-up conditions [1] and degradation [2]. Additionally, water flooding in the GDL can hinder the transport of waste heat, which can also result in performance losses [1]. The PEMFC is especially prone to flooding at high current densities and/or low flow stoichiometry [3].

Within the last few years, there has been a major thrust to use empirical methods to analyze the water distribution in PEMFCs through direct optical visualization [3–11], neutron imaging [1,12–19], and nuclear magnetic resonance imaging [20–24]. Liquid water visualizations have also been performed

with environmental scanning electron microscopy [25], gas chromatography [26], and microtomography [27]. Fluorescence microscopy has also been employed to obtain *ex situ* visualizations of water transport in the GDL [28,29]. Very recently, Manke et al. [30] employed synchrotron X-ray radiography to investigate the dynamics of liquid water formation in an operating PEMFC.

Liquid droplet formation and detachment in a gas flow channel has been studied using *ex situ* direct optical visualization [3,10,31] and recently using dynamic two-phase flow simulations [32,33]. There have also been a number of experiments with transparent PEMFCs in which liquid water has been directly visualized with digital photography [4–9,11]. Digital photography provides useful information on how flow field flooding corresponds to operating conditions, however, it does not afford the spatial resolution required to analyze the transport of liquid water within the GDL, which eventually leads to channel flooding.

Neutron imaging is an *in situ* technique and an attractive method for visualizing water content because of the neutron's sensitivity to hydrogen atoms in water [12] and insensitivity

to common fuel cell materials (for example, aluminum and graphite) [23]. Neutron imaging has provided useful quantitative measurements of liquid water accumulation in the PEMFC gas flow channels and GDL. In the past, neutron imaging did not provide the spatial resolution required to analyze the through-plane evolution of water transport [28]; however, the National Institute of Standards and Technology (NIST) has recently demonstrated the capability of imaging with a spatial resolution of 25 μm [34].

Feindel et al. [20,22–24] employed nuclear magnetic resonance (NMR) microscopy to investigate the production and distribution of water in an operating PEMFC. Tsushima et al. [21] also used NMR to study the membrane performance of an operating PEMFC with and without a supply of water. Although NMR provides useful information about the water content in the gas channels and membrane, it cannot resolve water content in the GDL due to the rapid attenuation of the signal in the carbon layer [24].

Nam and Kaviany [25] employed an environmental scanning electron microscope (ESEM) to visualize condensed water droplets on GDL fibers in the absence of bulk liquid water transport. This method provides high spatial resolution, however it is not possible to simulate fuel cell operating conditions. The authors proposed that micro-droplets agglomerate to form macro-droplets, which eventually flow preferentially toward larger pores. The authors hypothesized that water is distributed in a branching geometry where large streams act as the backbone for macro-transport, and smaller streams transport water from micro-droplets to macro-droplets. Pasaogullari and Wang [35] also hypothesized the formation of a tree-like liquid water percolation in the GDL after condensation begins.

Mench et al. [26] used gas chromatography to obtain *in situ* measurements of the water vapor distribution in PEMFC gas channels. Manke et al. [30] employed an *in situ* synchrotron X-ray radiography technique to observe the dynamic water transport behaviour in an operating PEMFC. They observed an *eruptive transport* mechanism [30], which they describe as the quick ejection of droplets from the GDL into the gas channel.

Our group [28] directly visualized through-plane liquid water transport in the GDL using a fluorescent tracer. A dye solution was injected through the gas diffusion layer of a PEMFC, and fluorescence microscopy was employed to visualize the transport of liquid water through this fibrous structure to the extent that the opaque fiber structure would allow. The technique allowed tracking of the time-evolving gas/liquid interfaces, and provided unique insight into the dynamics of liquid water flow through distinct pathways. Water transport at the surface was found to be dominated more by fingering and channeling, accompanied by highly dynamic eruptive water transport processes. Recent *in situ* visualizations using synchrotron X-ray radiography [30] confirm this eruptive transport process and show that this occurs during operation of some localized areas of the cell, while in others GDL pores fill continuously following the capillary tree-like process [25,35].

In this work, fluorescence microscopy is employed to investigate the dynamic liquid water transport behaviour in a simulated gas flow channel. A pressure transducer is employed to measure the liquid water pressure drop through the gas diffusion layer,
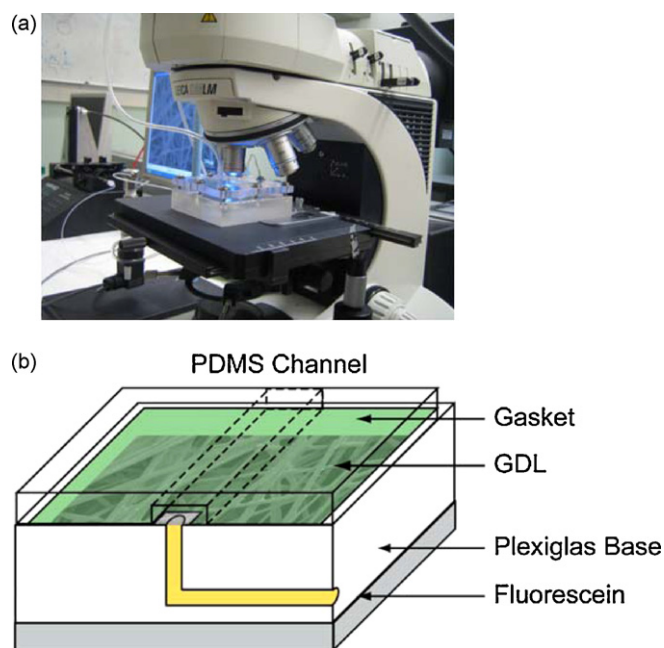
Fig. 1. Simulated gas flow channel apparatus: (a) photograph of gas flow channel apparatus on fluorescence microscope stage and (b) schematic showing the apparatus cross-section.

and these measurements together with fluorescence microscopy provide new insights into the dynamic effects of droplet emergence, departure and changing breakthrough locations.

2. Apparatus

Fig. 1 shows the experimental apparatus which consists of the gas flow channel apparatus on the fluorescence microscope stage and a schematic of the gas flow channel apparatus in cross-section. The GDL is placed between a Plexiglas base and a PDMS channel structure with dimensions (3.7 mm × 4.5 mm). The relatively large channel dimensions were chosen such that droplet emergence and transport could be studied in the absence of sidewall effects. A silicone rubber gasket was placed between the GDL and Plexiglas base to prevent leakage.

Air was delivered to the gas channel and controlled with a rotameter (Omega FL-3840G). Liquid water was injected through the bottom surface of the GDL using a syringe pump (Harvard Apparatus PHD 22/2000) connected to the the Plexiglas base with Teflon FEP tubing (Upchurch Scientific, WA). Unless otherwise stated, liquid was delivered at a rate of 0.005 mL min^{-1}. Assuming no net water transport between anode and cathode in a PEMFC, this water flow rate would correspond to high current density operation[1][3]. The liquid pressure

---

[1] Schulz et al. [36] argue that flow rates of this order correspond to unrealistically high current densities; however, this is not the case when considering the likelihood of discretely distributed sites of liquid water formation in a fuel cell. Under this consideration, the corresponding surface area with which a given water injection rate is associated would be larger than the masked water inlet area used in these *ex situ* experiments. Therefore, the liquid injection rates employed here are considered reasonable for the consideration of high current densities.

was measured with a pressure transducer (Omega PX4202-005G5V) with an operating range of 0–34 kPa. This pressure transducer was placed close to the Plexiglas base inlet. The pressure transducer was connected to a DAQ system (National Instruments, Austin, TX). The channel structure was cut from a PDMS layer. With a contact angle of $78°$, the PDMS channel is an appropriate material to simulate graphite bipolar plates with a contact angle of roughly $70–80°$ [6]. A Plexiglas top plate was clamped above with eight screws with a torque of $1 \, \text{in·lb screw}^{-1}$. An upright fluorescence microscope was used to capture the through-plane evolution of liquid water transport. To facilitate fluorescence imaging, fluorescein dye was used to tag the liquid phase (0.1 mM). The low dye concentration was used to ensure the physical properties of the solution effectively matched those of pure water [37]. Images were captured using a charge-coupled device (CCD) camera (Orca-AG, 12 bit) with a frame rate of 9.3 fps and binning of 4×4, resulting in a resolution of 325×257 pixels. Unless otherwise stated, all fluorescence images were obtained with a $5 \times$ magnification objective with a numerical aperture, $NA = 0.12$, and a spatial resolution of $8.14 \, \mu\text{m pixel}^{-1}$. Top view fluorescent images captured the evolution of liquid transport in the top few layers of the GDL, where the depth of optical access is limited by the opaque nature of the material.

In the work presented here, liquid water was introduced from one side of the GDL from a single localized source. The conditions imposed here, albeit simplified, provide insight into an operating fuel cell when considering the likelihood of distributed sites of liquid water formation in the cathode. Furthermore, with continuous liquid water formation in the catalyst layer or the lower layers of the GDL, liquid water will percolate through discrete locations of the GDL due to its porous and hydrophobic nature. However, these experiments do not capture the thermal gradients present in fuel cells, and the occurrence of condensation in the GDL may affect the behaviour of water transport observed in these experiments.

3. Results

3.1. Droplet growth

Fig. 2 shows the liquid water pressure measured as a function of time when water is injected at a constant rate of 0.005 mL min^{-1} with an average airflow velocity of $2 \, \text{m s}^{-1}$. After 20 min of liquid injection, the system reached a critical pressure, herein termed the *breakthrough pressure*, at which droplets began to appear on the surface of the GDL. The breakthrough pressure refers to the liquid water pressure required to penetrate through the cross-plane of an initially dry GDL. The *initial breakthrough* refers to the first appearance of a droplet on the surface of an initially dry GDL. In the pre-breakthrough period, the linearity of the pressure increase over time is mostly due to the expansion of the fluid delivery system. Post-breakthrough, individual droplets, which correspond to the pressure peaks, emerged and detached for the following 30 min. However, after 50 min, the gas channel became populated with water slugs, and individual droplets no longer appeared. This experiment
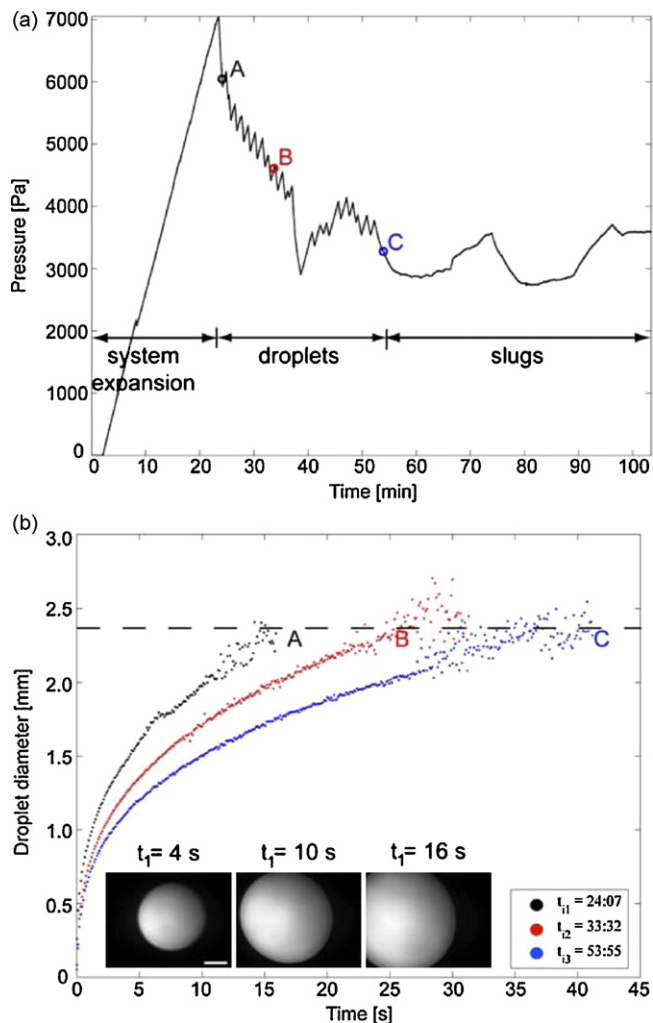
Fig. 2. Dynamic water transport behaviour through an initially dry GDL: (a) liquid water pressure showing the time periods in which single droplets emerged and detached from the GDL surface and in which slug formation led to channel flooding and (b) tracking the growth of three different droplets (A–C, which correspond to times shown in (a)) ($t = 0$ corresponds to incipient droplet formation). Raw fluorescence images are shown inset for the t_{i1} case at times indicated. Length bar indicates 0.5 mm.

is characteristic of several repeated trials, such that the initial breakthrough of liquid water in the GDL is preceded by a substantial growth of liquid water pressure, and breakthrough occurs when a critical pressure is reached.

The growth of individual droplets over time was tracked through image analysis. Fig. 2(b) shows the droplet diameter versus time for three individual droplets that emerged at the following three times: $t_{i1} = 24 : 07$ min, $t_{i2} = 33 : 32$ min, and $t_{i3} = 53 : 55$ min (also marked in Fig. 2(a)). All three droplets grow to approximately 2.4 mm in diameter before detaching from the GDL surface, however as time increases, the droplet takes longer to grow to that critical size. Fig. 2(b) (inset) shows a series of raw fluorescence images used to track the growth of the droplet for $t_{i1} = 24 : 07$ min. The dark portion of the images correspond to the GDL, and the bright white areas correspond to the liquid water. This figure shows that in the absence of pinning, the droplet reaches a critical size before detachment at a

given airflow velocity. However, the growth period required for the droplet to reach that size depends on how much time has passed since the initial breakthrough. When there is more liquid water pressure in the system, as there was at time 24:07 min, the droplet grows much more quickly than at later times when the pressure has significantly decreased.

In a typical fuel cell with channel geometry 0.5 mm × 0.5 mm, liquid droplets will clearly not reach the critical size observed here. However, these results indicate that droplets would also reach a critical size (albeit smaller) before detachment and experience similar pinning, with the same GDL material.

3.2. Droplet pinning

In all the experiments, individual droplets emerge, grow, and detach from the GDL. However, it was commonly observed that over time these droplets leave residual liquid water particles on the GDL, which provide pinning sites for other droplets. Droplets become pinned to the GDL due to its high surface roughness and high contact angle hysteresis. Under the same circumstances with a perfectly smooth and hydrophobic surface, a droplet may detach more easily and roll away from the breakthrough location as was shown numerically in [33]. The GDL surface consists on the other hand of randomly oriented carbon fibers with non-isotropic wettability. Droplets sitting on this highly rough surface experience fewer tendencies for detachment due to longer contact lines between the droplet and fibers and to the presence of contact angle hysteresis. Furthermore, residual water particles may also increase the tendency for droplet pinning. Typically, a transition occurred between individual droplet formation and detachment to slug formation, as shown in Fig. 2(a). Individual droplets then become pinned in the vicinity of the breakthrough location. They detach after subsequent droplets emerge and coalesce with the pinned droplet after reaching a critical size. Pinning affects droplet emergence frequency and size because before the droplet reaches its critical radius for departure, the droplet commonly coalesces with the pinned droplet. Fig. 3(a) is a raw image (top view) obtained from fluorescence microscopy showing the GDL pore (white) that is saturated with liquid at $t = 34 : 01$ min, and Fig. 3(b) is a raw image showing a spherical droplet sitting on top of the saturated pore that connects the droplet at $t = 34 : 03$ min. Due to the airflow from right to left, the droplet is shifted to the left. The contact line between the droplet and the GDL pore is shown in Fig. 3, which is defined by the saturated pore size. In contrast after several cycles of droplet detachment, Fig. 3(c) shows a pinned droplet at $t = 1$h 39min. The wetting contact line between the droplet and the GDL is no longer defined by the droplet's originating pore. Droplets emerge from a location directly to the right of the pinned droplet. These droplets detach at a much smaller critical size than described in Fig. 2. Once detached, these droplets immediately coalesce with the pinned droplet, contributing to an increasingly larger droplet. Although the GDL surface is hydrophobic and airflow velocities initially provide sufficient force to detach droplets, over time the GDL surface becomes prone to droplet pinning and eventual slug formation.
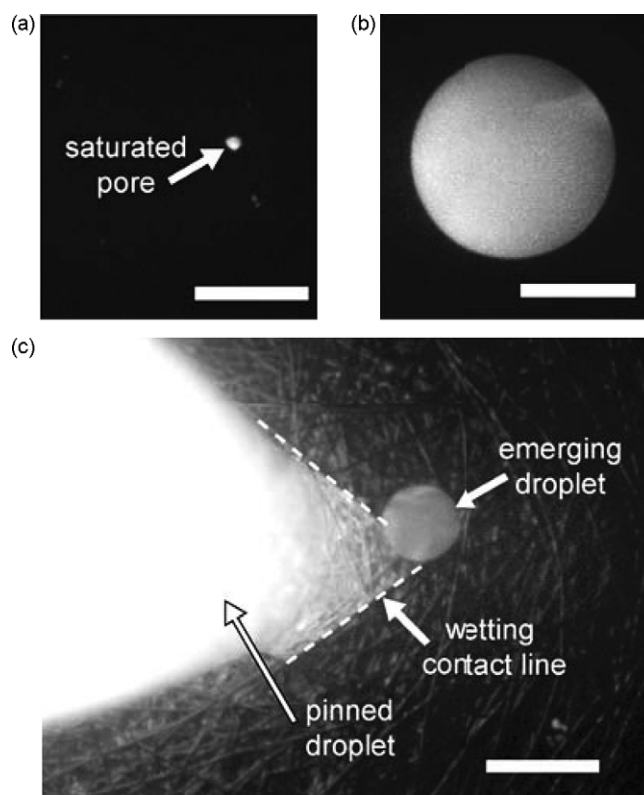
Fig. 3. Top view raw fluorescence images (white areas indicate location of liquid water) captured with a $2 \, \text{m s}^{-1}$ airflow velocity at (a) $t = 33 : 01$ min showing the saturated pore immediately prior to droplet emergence, (b) $t = 33 : 03$ min showing a droplet sitting above the saturated pore, and (c) after several droplet emergence/departure cycles showing a large droplet pinned to the GDL surface to the left of an emerging droplet. The airflow direction is from right to left, and the length bars are 0.5 mm long.

3.3. Dynamic breakthrough locations

It has been found that water emerges from the surface of the GDL in preferential locations corresponding to the path of least resistance [29]. Here, the determination of preferential water breakthrough locations was observed to be a dynamic process, i.e. the location of breakthrough changed over time. Observations suggest that new breakthrough locations arise due to a rearrangement of water pathways within the GDL. As a droplet is removed by airflow in the gas flow channel, the liquid pressure within the GDL continues to grow. During this pressure increase, it is conjectured that the interconnection of water pathways within the GDL evolves such that the preferential pathway for breakthrough may change. This rearrangement, typically accompanied by a pressure increase, would then be followed by a drop in pressure associated with a quick succession of droplets. Such behaviour is consistent with the *ex situ* observations of Litster et al. [28] and the recent *in situ* measurements of Manke et al. [30], who termed the phenomenon as *eruptive transport*. This eruptive transport can be explained by the pressure increase measured in this work. It was observed that when a new breakthrough location forms, the old breakthrough location can be seen to recede (shown in Fig. 4), which suggests the extent of branching within the GDL. Fig. 4 shows the
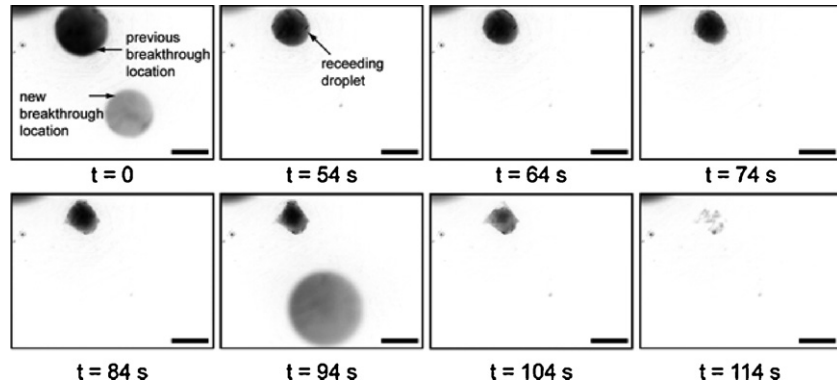
Fig. 4. Time series of fluorescence images showing the recession of a droplet formed above the previous breakthrough location. A new breakthrough location has emerged in the lower right hand corner of field of view. The images have been inverted for clarity, and length bars represent 0.5 mm.
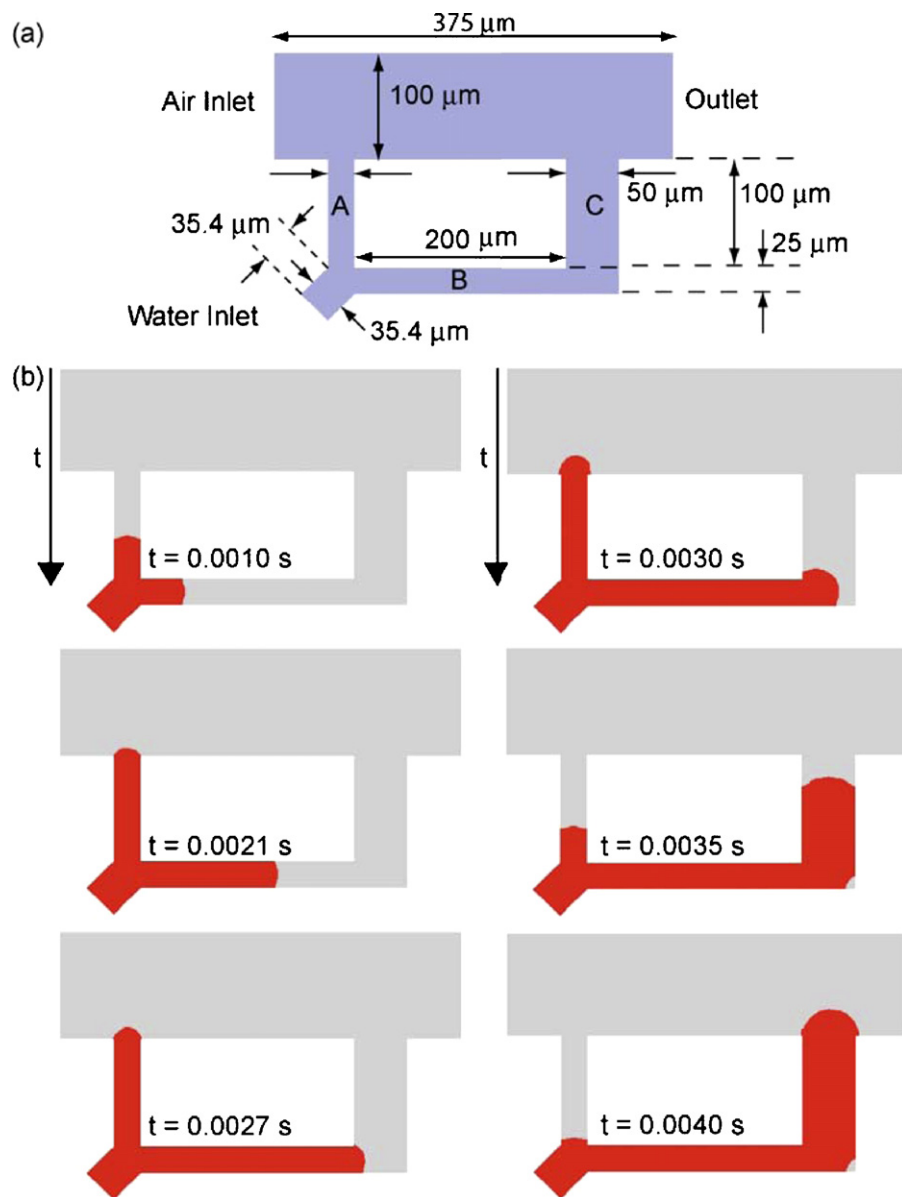
Fig. 5. Volume of fluid (VOF) simulations results: (a) schematic showing the computational domain of the gas flow channel with two GDL pores (channels A and C) and (b) time series of VOF simulation results showing the primary filling of the smaller channel (A) followed by the secondary filling of the larger channel (C) (red represents liquid water, and gray represents air). (For interpretation of the references to color in this figure legend, the reader is referred to the web version of the article.)

time evolution of changing breakthrough locations over a period of approximately 2 min. The first frame ($t = 0$ s) shows the droplet that emerged from a preferential breakthrough location, and at the same time a droplet emerged from a new breakthrough location (lower right). As several droplets emerge and depart from the new location, the droplet sitting at the top of the viewing area recedes until only traces are visible at $t = 114$ s. Although channeling has been recently proposed to be the dominant mechanism of water transport in the GDL, these new results suggest that it is a combination of channeling with the growth of an interconnected dynamic network of water pathways within the GDL that dominates the mechanism of water transport.

3.4. Volume of fluid simulations

To better understand and highlight the driving mechanisms, computational fluid dynamics (CFD) modelling was performed with the volume of fluid method using the commercial CFD package, FLUENT 6.2.16. The volume of fluid method, developed by Hirt and Nichols [38] is a popular method of solving time-dependent flows by applying a surface-tracking technique (see Zhu et al. [32] for more details). Fig. 5(a) illustrates the idealized two-dimensional computational domain, which consists of a $375\,\mu$m $\times$ $100\,\mu$m gas flow channel. The air inlet is at the left boundary, and the two phase outlet is at the right boundary. Two microchannels, A and C ($25\,\mu$m $\times$ $100\,\mu$m and $50\,\mu$m $\times$ $100\,\mu$m, respectively), are connected by a $25\,\mu$m $\times$ $200\,\mu$m horizontal channel (B). Channels A and C are connected to the gas flow channel. A structured orthogonal computational mesh consisting of 2,164 cells was used. The adequacy of this grid was tested by increasing the number of grid nodes by 100%, and similar transport processes were obtained. Simulations were performed with time steps of 10^{-7} s. A no-slip boundary condition was imposed along the walls of the domain. A contact angle of $70°$ was set for the top wall, and $140°$ for the bottom wall and the microchannels that simulate GDL pores. The airflow velocity was set to $10\,\mathrm{m\,s^{-1}}$ at 100 kPa, and liquid water was injected at a velocity of $0.1\,\mathrm{m\,s^{-1}}$. Fig. 5(b) shows the time evolution of channel filling connected to a gas channel. At $t = 0.0010$ s, both $25\,\mu$m channels (A and B) fill simultaneously. However, when channel A becomes completely filled, the capillary force required to form a droplet exceeds the threshold capillary force required for the pathway in channel B to continue filling the horizontal channel. Thus, channel B continues to fill with liquid water. Once the pathway in channel B reaches the larger pore (C), liquid water flows into channel C while flowing out of channel A. The liquid height in channel A recedes, and the larger channel (C) provides the breakthrough location for the first droplet. The time evolution of water transport between two competing channels shows that in the presence of an interconnected pathway of water channels, dominating preferential pathways can lead to the recession of intial pathways. The observations described in Fig. 4 supported by these CFD VOF simulations shown in Fig. 5 help explain the dynamic fingering and *eruptive transport* mechanisms [28,30].

4. Conclusions

The dynamic water transport behaviour in and on the surface of the GDL was explored with experimental and numerical methods. With a combination of fluorescence microscopy and liquid pressure drop measurements, it was found that with an initially dry GDL and gas channel apparatus, the emergence and detachment of individual droplets was followed by slug formation and channel flooding. With an initially dry GDL, the pore that defines the contact line between a spherical droplet and the GDL surface is quite small. After the GDL surface has been exposed to droplet particles, the surface becomes prone to droplet pinning and flooding. Droplets become pinned to the GDL's rough surface with large wetting contact lines, and much higher airflow rates are needed to remove these pinned droplets. The changing breakthrough location suggests a dynamic and interconnected network of water pathways within the GDL, which is supported by numerical results from an idealized test system simulating the filling behaviour of liquid water within two competing pathways. These simulations showed that once a new preferential pathway is found, less preferable pathways recede. These results support the experimental observations of receding droplets. The work presented in this paper provides insight into the changing behaviour of liquid water transport in the GDL when operating under nominally static conditions.

References

[1] J.J. Kowal, A. Turhan, K. Heller, J. Brenizer, M.M. Mench, Journal of the Electrochemical Society 153 (10) (2006) A1971–A1978.
[2] A. Taniguchi, T. Akita, K. Yasuda, Y. Miyazaki, Journal of Power Sources 130 (2004) 42–49.
[3] E.C. Kumbur, K.V. Sharp, M.M. Mench, Journal of Power Sources 161 (2006) 333–345.
[4] K. Tüber, D. Pócza, C. Hebling, Journal of Power Sources 124 (2003) 403–414.
[5] A. Hakenjos, H. Muenter, U. Wittstadt, C. Hebling, Journal of Power Sources 131 (2004) 213–216.
[6] X.G. Yang, F.Y. Zhang, A.L. Lubawy, C.-Y. Wang, Electrochemical and Solid-State Letters 7 (11) (2004) A408–A411.
[7] J. Borrelli, S.G. Kandlikar, T. Trabold, J. Owejan, Proceedings of the 3rd International Conference on Microchannels and Minichannels, June 13–15, 2005, p. ICMM2005-75118.
[8] K. Sugiura, M. Nakata, T. Yodo, Y. Nishiguchi, M. Yamauchi, Y. Itoh, Journal of Power Sources 145 (2005) 526–533.
[9] D. Spernjak, S. Advani, A.K. Prasad, Proceedings of the ASME 4th International Conference on Fuel Cell Science, Engineering and Technology, 2006, FUEL CELL2006-97271.
[10] A. Theodorakakos, T. Ous, M. Gavaises, J.M. Nouri, N. Nikolopoulos, H. Yanagihara, Journal of Colloid and Interface Science 300 (2006) 673–687.
[11] F.-B. Weng, A. Su, C.-Y. Hsu, C.-Y. Lee, Journal of Power Sources 157 (2006) 674–680.

[12] R. Satija, D.L. Jacobson, M. Arif, S.A. Werner, Journal of Power Sources 129 (2004) 238–245.

[13] D. Kramer, E. Lehmann, G. Frei, P. Vontobel, A. Wokaun, G.G. Scherer, Nuclear Instruments and Methods in Physics Research A 542 (2005) 52–60.

[14] D. Kramer, J. Zhang, R. Shimoi, E. Lehmann, A. Wokaun, K. Shinohara, G.G. Scherer, Electrochimica Acta 50 (2005) 2603–2614.

[15] N. Pekula, K. Heller, P.A. Chuang, A. Turhan, M.M. Mench, J.S. Brenizer, K. Unlu, Nuclear Instruments and Methods in Physics Research A 542 (2005) 134–141.

[16] T.A. Trabold, J.P. Owejan, D.L. Jacobson, M. Arif, P.R. Huffman, International Journal of Heat and Mass Transfer 49 (2006) 4712–4720.

[17] J.P. Owejan, T.A. Trabold, D.L. Jacobson, D.R. Baker, D.S. Hussey, M. Arif, International Journal of Heat and Mass Transfer 49 (2006) 4721–4731.

[18] A. Turhan, K. Heller, J.S. Brenizer, M.M. Mench, Journal of Power Sources 160 (2006) 1195–1203.

[19] J. Zhang, D. Kramer, R. Shimoi, Y. Ono, E. Lehmann, A. Wokaun, K. Shinohara, G.G. Scherer, Electrochimica Acta 51 (2006) 2715–2727.

[20] K.W. Feindel, L.P.-A. LaRocque, D. Starke, S.H. Bergens, R.E. Wasylishen, Journal of the American Chemical Society 126 (2004) 11436–11437.

[21] S. Tsushima, K. Teranishi, K. Nishida, S. Hirai, Magnetic Resonance Imaging 23 (2005) 255–258.

[22] K.W. Feindel, S.H. Bergens, R.E. Wasylishen, Journal of the American Chemical Society 128 (2006) 14192–14199.

[23] K.W. Feindel, S.H. Bergens, R.H. Wasylishen, ChemPhysChem 7 (2006) 67–75.

[24] K.W. Feindel, S.H. Bergens, R.E. Wasylishen, Physical Chemistry Chemical Physics (2007) 1–17.

[25] J.H. Nam, M. Kaviany, International Journal of Heat and Mass Transfer 46 (2003) 4595–4611.

[26] M.M. Mench, Q.L. Dong, C.-Y. Wang, Journal of Power Sources 124 (2003) 90–98.

[27] P.K. Sinha, P. Halleck, C.-Y. Wang, Electrochemical and Solid-State Letters 9 (7) (2006) A244–A348.

[28] S. Litster, D. Sinton, N. Djilali, Journal of Power Sources 154 (2006) 95–105.

[29] A. Bazylak, D. Sinton, Z.-S. Liu, N. Djilali, Journal of Power Sources 163 (2007) 784–792.

[30] I. Manke, Ch. Hartnig, M. Grünerbel, W. Lehnert, K. Kardjilov, A. Haibel, A. Hilger, J. Banhart, H. Riesemeier, Applied Physics Letters 90 (2007) 174105–1741053-1741053.

[31] C.H. Hidrovo, F.-M. Wang, J.E. Steinbrenner, E.S. Lee, S. Vigneron, C.-H. Cheng, J.K. Eaton, K.E. Goodson, Proceedings of the ASME 3rd International Conference on Microchannels and Minichannels, 2005, p. ICMM2005-75261.

[32] X. Zhu, P.C. Sui, N. Djilali, Microfluidics Nanofluidics, in press, [doi:10.1007/s10404-007-0209-9].

[33] X. Zhu, P.C. Sui, N. Djilali, Journal of Power Sources 127 (2007) 287–295.

[34] D.S. Hussey, D.L. Jacobson, M. Arif, J.P. Owejan, J.J. Gagliardo, T.A. Trabold, Journal of Power Sources 172 (2007) 225–228.

[35] U. Pasaogullari, C.-Y. Wang, Journal of the Electrochemical Society 151 (3) (2004) A399–A406.

[36] V.P. Schulz, J. Becker, A. Wiegmann, P.P. Mukherjee, C.-Y. Wang, Journal of The Electrochemical Society 154 (4) (2007) B419–B426.

[37] H. Anderson, S. Fu, T.G. Myers, C.P. Thompson, Proceedings of the 9th International Symposium On Flow Visualization, Paper 8, 2000, p. 1–7.

[38] C.W. Hirt, B.D. Nichols, Journal of Computational Physics 39 (1) (1981) 201–225.